

## Brad Paden

Department of Mechanical and Environmental  
Engineering,  
University of California,  
Santa Barbara, CA 93106  
e-mail: paden@engineering.ucsb.edu

## Nelson Groom

NASA LARC (ret.),  
P.O. Box 125, White Marsh, VA 23183  
e-mail: njgroom@visi.net

## James F. Antaki

Biomedical Engineering,  
Carnegie Mellon University,  
Pittsburgh, PA 15213  
e-mail: antaki@andrew.cmu.edu

# Design Formulas for Permanent-Magnet Bearings

*As the energy densities in permanent magnet materials increases, permanent magnet (PM) bearings are becoming increasingly attractive machine elements for applications ranging from turbo machinery to energy storage flywheels. Desirable qualities include high speed, low wear, energy savings, and freedom from lubricants that can degrade or contaminate other system components. In this paper we develop analytical expressions for stiffness and peak load in stacked-structure radial magnetic bearings that extend the seminal work of Backers, and Yonnet and co-workers. In addition to the derivation of simple design rules, the axial peak force and negative axial stiffness are calculated. [DOI: 10.1115/1.1625402]*

**Keywords:** Permanent Magnet Bearings, Machine Elements, Design Formulas

## 1 Introduction

The development of high-energy product permanent magnet (PM) materials has made PM magnetic bearings an attractive option for applications ranging from turbo machinery to energy-storage flywheels. In small high-speed turbo compressors, bearing longevity is a problem that can be resolved with PM magnetic bearings. In space instrument applications, magnetic bearings eliminate the need for lubricants, which can contaminate optical surfaces; and in energy-storage flywheels, PM magnetic bearings allow operation in a vacuum. In this paper a radial magnetic bearing configuration, shown in Fig. 1(a), is studied in detail, and a result of Yonnet [1] is applied to show that the governing equations also hold for the axially magnetized bearing depicted in Fig. 2. The objective is to derive simple design relationships that will make magnetic bearings accessible to the non-specialist designer. Peak bearing load and bearing stiffness, normalized by bearing axial cross-sectional area, are the key performance measures useful to mechanical engineers, and new analytical expressions are derived for these quantities. PM bearings compete with feedback-controlled active magnetic bearings in many designs. Active magnetic bearings have the advantage of higher stiffness, higher loads and better damping, and are capable of active vibration isolation and fine positioning in rotating machinery. However, active bearings can cost many times more than comparable PM bearings. The stiffness levels in PM bearings can be improved provided many thin PM magnets are stacked together as the analysis herein shows. The benefit of lubricant-free operation is accompanied by the drawback of poor damping in the absence of liquid in the gap; thus PM bearings can be particularly attractive for use in liquid pumps. Incorporating eddy-current dampers can also increase damping. PM bearings have been used in turbo molecular pumps, and are being used in artificial hearts [2].

As a consequence of Earnshaw's theorem, it is not possible to levitate a body statically solely with permanent magnets in a static magnetic field. Indeed, a radial PM bearing has a negative axial stiffness, which has twice the magnitude of the radial stiffness. As a consequence, PM bearings are always used in conjunction with other bearings. In the case of radial PM bearings, there is often an active thrust magnetic bearing used for positioning in the axial direction.

**Historical Perspective.** Baermann [3] invented the PM magnetic bearing in 1954, and Backers [4] performed the first detailed

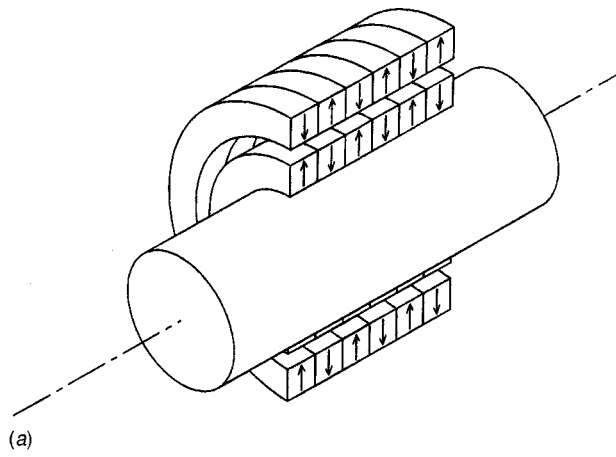
analysis and experimental verification in 1960–1961 at Philips Laboratories. Since that early development work, there has been widespread development and application of permanent magnet bearings. Yonnet and his co-workers [1,5,6] have developed basic analysis methods and applied them to a wide variety of radial magnetic bearings and couplings. In contrast to Backers use of the scalar magnetic potential, Yonnet used interactions of differential magnetic dipoles to formulate force and stiffness expressions which are integrals of the interactions amongst rotor and stator elements. The purpose of the dipole interaction approach is to capitalize upon certain symmetry properties of magnetic bearing design that become apparent with the technique. Recently, Marinescu and Marinescu [7] have developed a perturbation method for stiffness calculation in permanent magnetic bearings that employs a surface current model, which differs from the approaches of both Backers and Yonnet.

In this paper the formulation of Backers is followed closely and extended by replacing a numerical integration with a closed-form expression to yield analytical expressions for radial force and stiffness characteristics of PM bearings. The symmetry results of Yonnet's dipole interaction approach also lead us to conclude that the force and stiffness characteristics of bearings in Figs. 1(a) and 2 are identical. In addition, new axial force and stiffness expressions are given to aid designers in determining thrust bearing requirements. The force expressions are derived using Backers' formula for the interaction of two sinusoidally magnetized plates together with a Fourier expansion of the magnetization in a stacked magnet structure. The expression for the peak load is then computed for the bearing structure in Fig. 1 with the stack end-effects neglected.

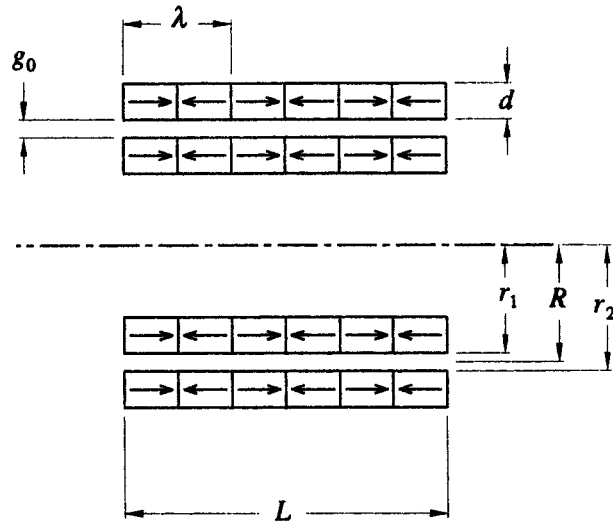
The radial load expression is evaluated to observe that for neodymium-iron-boron with a remanence of 42 megaGauss-Oersted, the peak load capacity is 0.42 Mpa, or 60 psi, times the axial cross sectional area of the bearing ( $=2RL$  in Fig. 1(b)). A useful rule-of-thumb for the associated radial stiffness is 60 psi/radial gap, where the minimum radial gap (and maximum stiffness) is determined by manufacturing and operating limitations.

In section 2, Backers' derivation of the magnetic potential energy in adjacent sinusoidally magnetized plates is summarized and expanded to include the case of plates magnetized in a square wave. This review is necessary as we use intermediate results of Backers' derivation in calculating axial force characteristics of the bearing. In Section 3, the application of the magnetic potential energy formula is made to a radial magnetic bearing, and a closed-form expression for the load characteristics of sinusoidally mag-

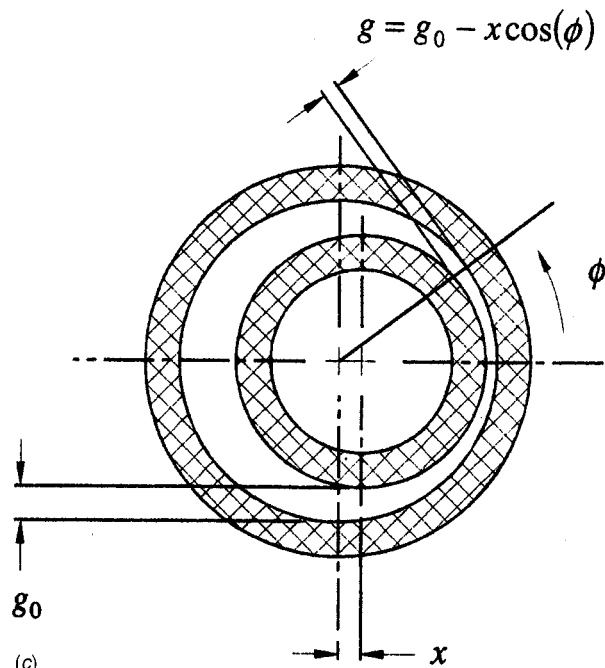
Contributed by the Mechanisms and Robotics Committee for publication in the JOURNAL OF MECHANICAL DESIGN. Manuscript received March 2003; revised April 2003. Associate Editor: J. Michael McCarthy.



(a)



(b)



(c)

Fig. 1 Magnetic bearing geometry with load; (a) isometric view, (b) axial cross-section and, (c) radial cross-section

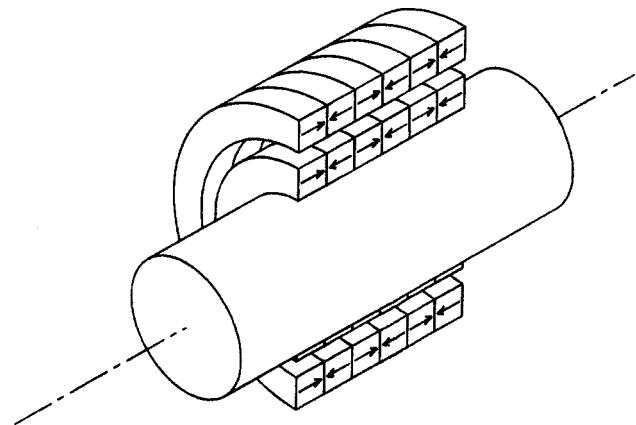


Fig. 2 An axially magnetized bearing has same load capacity and stiffness as the bearing in Fig. 1 (See [1])

netized radial bearings is presented. The sinusoidal result is used in conjunction with the Fourier series to obtain a series expansion for the load characteristics of a stacked radial bearing. The series is differentiated to find the stiffness. The axial load characteristics are developed in section 4, and conclusions are made in section 5.

## 2 Interaction of Sinusoidally Magnetized Plates

We begin our analysis by summarizing Backers' calculation of the interaction forces between the two infinite and periodically magnetized plates of thickness  $d$  depicted in Fig. 3. His intermediate calculations are included in addition to the final formula since we use one of his intermediate results for the axial force derivation in section 4. We expound on his work by describing the case where the plates are magnetized at different frequencies. Backers' basic result will enable the analysis of other periodic systems through the use of Fourier expansions. Following the formulation of Backers, we let plate C in Fig. 3 be located parallel to the  $x$ - $z$  plane of a right-handed coordinate frame (only the  $x$  and  $y$  axes are shown) and let plate C occupy the region defined by  $y \in (-d, 0)$ . A second plate, B is also parallel to the  $x$ - $z$  plane, but is separated from plate C by a gap  $g$  and occupies the region  $y \in (g, g+d)$ . Plates B and C are periodically magnetized in the  $y$  direction according to

$$M_C = M_0 \cos(m2\pi z/\lambda). \quad (1)$$

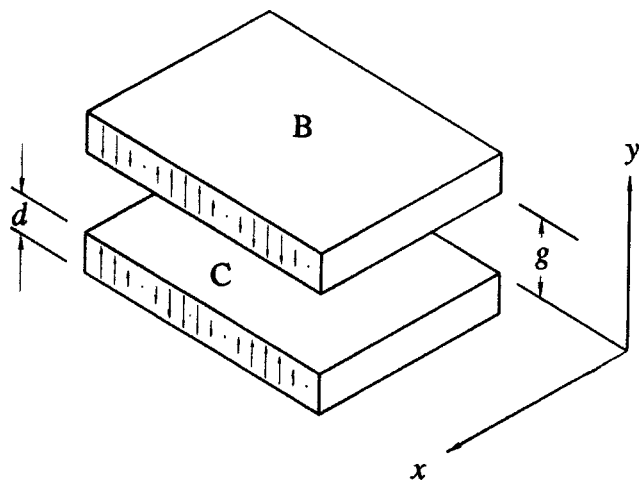


Fig. 3 Geometry of interacting periodically magnetized plates showing direction of magnetization

The magnetization  $M$  is given by  $M=B-\mu H$ . The frequency is  $m/\lambda$  cycles per meter where  $m \in \{1,2,3 \dots\}$ . In the case that the PM material is saturated during the magnetization process,  $M_0$  is equal to the remanence  $B_r$  of the material. Plate B is magnetized with the same amplitude, but with a different periodic magnetization and phase. Let the spatial frequency be  $n/\lambda$ , where  $n \in \{1,2,3 \dots\}$  and the phase shift be captured by a displacement  $z_0$ . Hence

$$M_B = M_0 \cos(n2\pi(z+z_0)/\lambda). \quad (2)$$

The scalar magnetic potential at a point  $(x,y,z)$  due to plate C is given by

$$U(x,y,z) = \frac{1}{4\pi\mu_0} \int_{V_C} \frac{M_C \cdot \mathbf{r}}{r^3} dV. \quad (3)$$

Where  $\mathbf{r}$  is the position vector  $\{x,y,z\}^T$  and  $M_C$  is the magnetization of plate C. Due to the  $1/r^3$  in the integrand the integral is finite. The magnetic field is then given by  $\mathbf{H} \equiv \{H_x, H_y, H_z\}^T = -\nabla U$ .

$$\sigma_y = \begin{cases} -\frac{M_0^2}{4\mu_0} (1 - e^{-2\pi d/\lambda})^2 e^{-2\pi g/\lambda} \cos(n2\pi z_0/\lambda) & \text{if } m=n \\ 0 & \text{if } m \neq n \end{cases}. \quad (6)$$

The latter orthogonality result, that the interaction of periodically magnetized plates is zero when the periods are not equal, makes the calculation of interaction forces for stacked structures rather simple. This completes Backers' derivation. In the next section a new closed-form expression for the force-displacement characteristics for the PM stacked structure of Fig. 1 is derived for the assumption of negligible end-effects (i.e.  $L \gg \lambda$ ).

### 3 Normalized Radial Stiffness and Peak Load

In this section the configuration of Fig. 1 is analyzed under the assumptions that the  $R \gg d$ ,  $L \gg \lambda$ , and the  $y$  magnetization is sinusoidal along the  $z$  direction with wavelength  $\lambda$ . The two-dimensional repulsive force per unit area is calculated for each differential arc  $Rd\phi$  (see Fig. 1(c)) since  $R \gg d$ . The cosine term in Backers' equation is minimized at  $z_0 = \lambda/2$ . Accordingly, this value is chosen to maximize the repulsive force between the two magnet plates. Next, remove the assumption of sinusoidal magnetization by expanding a square-wave magnetization field as a Fourier series, and applying the formula (6) to each term. From the symmetry of the configuration shown in Fig. 1(a) we see that the restoring force is zero in the  $y$  direction.

For the radial bearing with nominal gap  $g_0$ , and displacement  $x$  due to loading, the clearance  $g(\phi)$  around the bearing is easily seen to be

$$g = g_0 - x \cos(\phi). \quad (7)$$

Substituting this expression for  $g$  in Backers' Formula, and integrating over the plate area yields the projection of the radial force on the  $x$  direction:

$$F = \frac{LRM_0^2}{4\mu_0} (1 - e^{-2\pi d/\lambda})^2 e^{-2\pi g_0/\lambda} \int_{-\pi}^{\pi} e^{-2\pi x/\lambda \cos \phi} \cos \phi d\phi. \quad (8)$$

Recognizing that this integral can be expressed in terms of an  $n$ th order modified Bessel function of the first kind (commonly denoted as  $J_n$  [8]) and normalizing by the area  $2LR$ , we have the force equation for the sinusoidal magnetized radial bearing,

The potential energy of a volume  $V_B$  of plate B in the field of plate C is

$$E = - \int_{V_B} \mathbf{H} \cdot \mathbf{M}_B dV = - \int_{V_B} H_y M_B dV. \quad (4)$$

By taking the volume  $V_B$  to be a rectangular region with its  $z$ -dimension an integer multiple of  $\lambda$ , its  $y$ -dimension to be  $d$  and its  $x$ -dimension to be an arbitrary width  $w > 0$ , the repulsive force per unit area is then

$$\sigma_y = \frac{-1}{w\lambda} \frac{\partial E(\lambda, w)}{\partial y}. \quad (5)$$

By the calculus of residues, we obtain Backers' Formula [4]:

$$\frac{F}{2LR} = \frac{\pi M_0^2}{4\mu_0} (1 - e^{-2\pi d/\lambda})^2 e^{-2\pi g_0/\lambda} I_1(2\pi x/\lambda). \quad (9)$$

Note that all length parameters appear normalized by  $\lambda$ . As a consequence, all the design parameters are conveniently expressed as dimensionless quantities.

Next, a Fourier expansion is taken of the radial magnetization (see Fig. 4) of the stacked structure of Fig. 1. With the assumption that the permanent magnet rings are fully magnetized to  $B_r$ , the remanence of the material can be expressed as

$$M_B(z) = -M_C(z) = \frac{4B_r}{\pi} \sum_{n=1,3,5 \dots} \frac{1}{n} \cos(n2\pi z/\lambda). \quad (10)$$

Owing to the orthogonality property in Eq. (6), the individual effects of each term in the sequence can be summed directly using Eq. (9) to yield an effective pressure on the journal cross sectional area  $2LR$  of

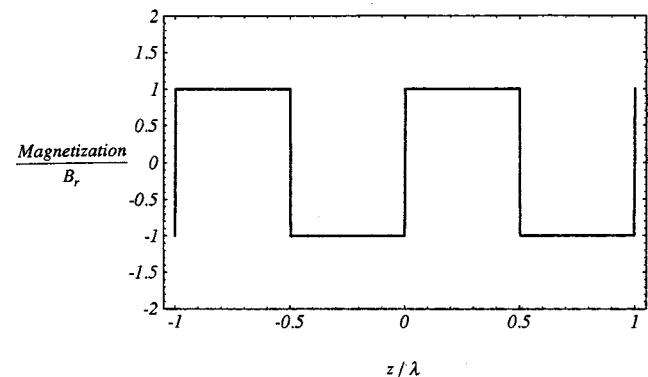


Fig. 4 Magnetization pattern in the stacked structure of Fig. 1.  $B_r$  is the remanence of the permanent magnet material,  $\lambda$  is the spatial period of the bearing pole pattern, and  $z$  is the displacement along the axis of the bearing.

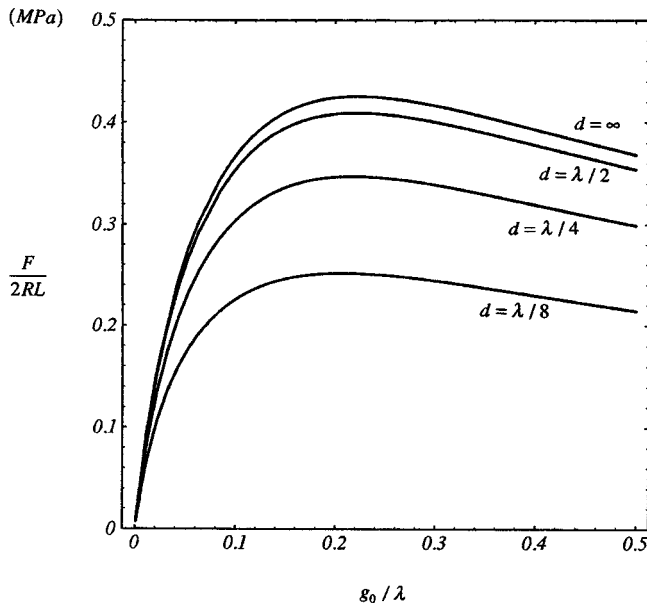


Fig. 5 Radial peak force versus normalized gap for bearings of Figs. 1 and 2;  $d/\lambda=1/8,1/4,1/2,\infty$ ;  $B_r=1.3$  Tesla

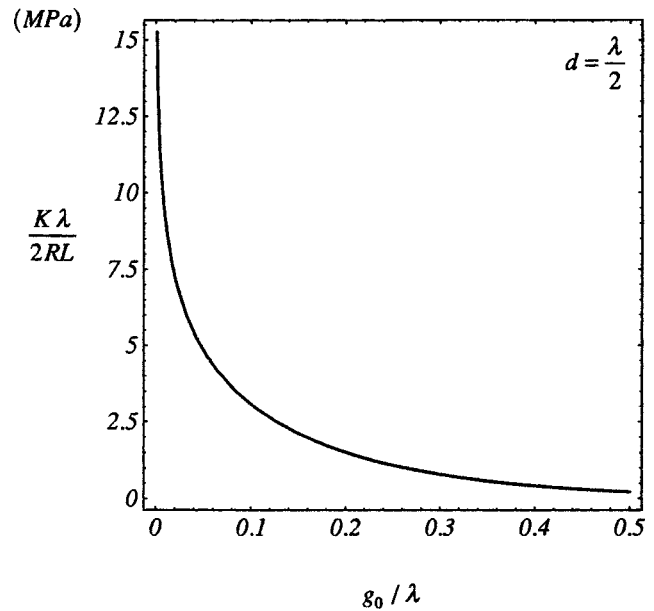


Fig. 7 Radial stiffness as a function of nominal gap  $d/\lambda=1/2$ ;  $B_r=1.3$  Tesla

$$\frac{F(x,g,d)}{2LR} = \frac{4B_r^2}{\pi\mu_0} \sum_{\substack{n=1 \\ \text{odd}}}^{\infty} \frac{1}{n^2} (1 - e^{-n2\pi d/\lambda}) e^{-n2\pi g/\lambda} I_1(n2\pi x/\lambda). \quad (11)$$

The magnetic pressure increases with the radial thickness  $d$  of the rings via the factor  $(1 - e^{-n2\pi d/\lambda})$  in Eq. (11). Note that this factor quickly approaches 1 as  $d$  is increased and little additional load capability is gained for  $d > \lambda$ . This is an important parameter in design since the volume (mass) of the PM material requirement grows linearly with  $d$ . Moreover, the summation converges rapidly and the first few terms in the summation are all that are required for most design calculations.

Consider the objective of choosing  $g$  and  $d$  to provide maximal force at full deflection corresponding to rotor-stator contact (i.e.

$x=g$ ). Setting  $x=g$ , and plotting  $F/2RL$  for various values of radial thickness yields the characteristic curves in Fig. 5. The optimal value of  $g/\lambda$ , obtained numerically from Eq. (11) is 0.22 and is a bit higher than the  $1/2\pi \approx 0.16$  suggested in [4]. Note that setting  $d=\lambda/2$  (i.e. rings with square cross section) achieves 96% of the limiting value with  $d=\infty$ . The limiting loading can be evaluated and is given by

$$\frac{F(.22,.22,\infty)}{2LR} = 1.26 \frac{B_r^2}{4\mu_0}, \quad (12)$$

where the factor 1.26 compares with 1.20 obtained by Backers with a numerical integration of Eq. (9). Evaluating this expression for neodymium-iron-boron with a remanence of 1.3 Tesla (42 MGOe) leads to a limiting load of 0.424 MPa (60.4 psi). When  $d=\lambda/2$  the peak load drops only four percent to 0.401 MPa or 58.1 psi.

Figure 6 shows the dependence of Eq. (11) on radial deflection for various gaps  $g_0$ . Note that for small gaps the bearing force characteristic is quite linear, but for large gaps the characteristic is that of a stiffening spring.

Differentiating the force expression (11) with respect to  $x$  and evaluating at  $x=0$  yields an expression for the nominal stiffness of the bearing:

$$K \equiv \left. \frac{\partial}{\partial x} \right|_{x=0} \frac{F(x,g,d)}{2LR} \quad (13)$$

$$= \frac{4B_r^2}{\lambda\mu_0} \sum_{\substack{n=1 \\ \text{odd}}}^{\infty} \frac{1}{n} (1 - e^{-n2\pi d/\lambda}) e^{-n2\pi g/\lambda}. \quad (14)$$

A plot of the stiffness as a function of  $g/\lambda$  with  $d=\lambda/2$  is provided in Fig. 7 and one can see that very high stiffnesses are possible. However, high stiffness is achieved at the cost of tight gap tolerances and many thin rings in a stack.

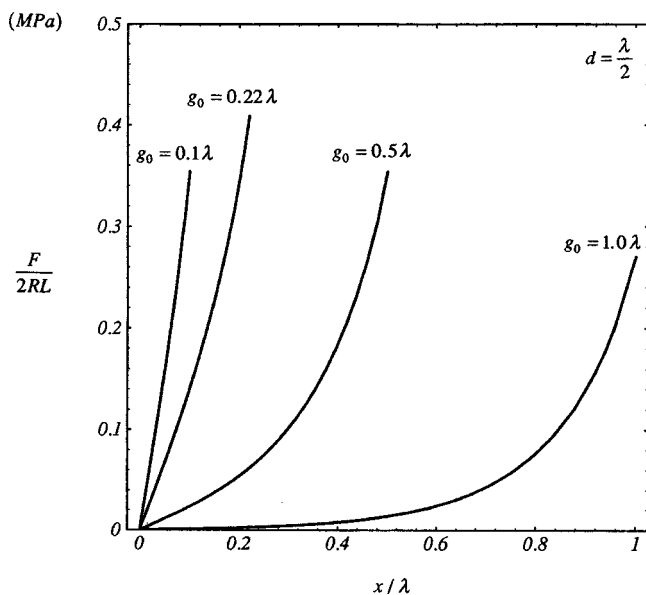


Fig. 6 Radial restoring force versus displacement for bearings of Figs. 1 and 2;  $d/\lambda=1/2$ ;  $g_0/\lambda=0.1,0.22,0.5,1.0$ ;  $B_r=1.3$  Tesla

#### 4 Axial Stiffness and Force

By differentiating the magnetic potential energy Eq. (3) with respect to  $z$ , the normalized axial force can be derived in a fashion similar to the radial force Eq. (11):

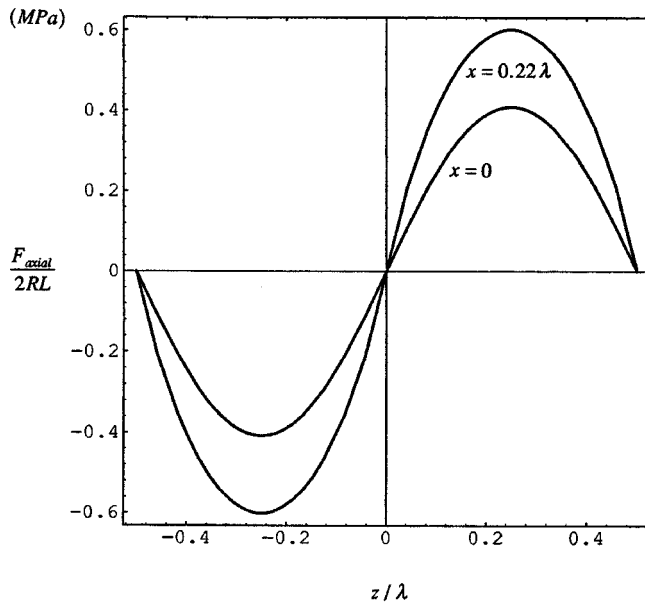


Fig. 8 Axial force as a function of axial displacement for two values of the radial displacement  $x$  ( $d=\lambda/2$ ,  $g=0.22\lambda$ ,  $B_r=1.3$  Tesla)

$$F_{axial}(z,x,g,d) = \frac{4B_r^2}{\pi\mu_0} \sum_{\substack{n=1 \\ \text{odd}}}^{\infty} \frac{1}{n^2} (1 - e^{-n2\pi d/\lambda}) \times e^{-n2\pi g/\lambda} I_0(n2\pi x/\lambda) \sin(n2\pi z/\lambda). \quad (15)$$

When the radial force was derived previously,  $z$  was set equal to  $\lambda/2$  to maximize the peak load and stiffness. Here, the radial dependence of the axial load is carried throughout the calculation. The modified Bessel function  $I_0$  is even and monotonically increasing for positive arguments, so the worst-case axial load occurs at  $x=g$ . The axial force for the  $x=0$  and  $x=g$  cases are plotted in Fig. 8 for  $d=\lambda/2$ ,  $g=0.22\lambda$ . These axial forces must be overcome by an active thrust system. Consequently, an active thrust system can be sized based on this equation. Figure 8 suggests as a design rule-of-thumb 0.6 MPa (85 psi) for the peak axial pressure where the force is calculated by multiplying by  $2RL$ .

The axial stiffness is negative when the radial bearing is properly aligned and is calculated by differentiating Eq. (15) with respect to  $z$  and evaluating at  $(x,z)=(0,0)$ :

$$K_{axial} \equiv \left. \frac{\partial}{\partial z} F_{axial}^*(z,x,g,d,\lambda) \right|_{x,z=0} = -\frac{8B_r^2}{\lambda\mu_0} \ln \left( \sqrt{\frac{e^{4\pi g/\lambda} - 1}{e^{4\pi(d+g)/\lambda} - 1}} \frac{e^{2\pi(d+g)/\lambda} - 1}{e^{2\pi g/\lambda} - 1} \right). \quad (16)$$

Observe that the axial stiffness is minus twice the radial stiffness. This is a direct consequence of Earnshaw's theorem. For a permanent magnet system in a static magnetic field, the eigenvalues of

the stiffness matrix will always add up to zero. In this case there are two radially directed eigenvectors and one axially directed eigenvector of the stiffness matrix.

## 5 Conclusions

Closed form solutions for the radial and axial stiffnesses were obtained for two radial bearing configurations. The results useful to machine designers are the curves in Figs. 5, 6, 7 and 8, and the corresponding design Eqs. (11) and (15). As seen in Eq. (11), increasing the radial thickness  $d$  of the bearing increases the bearing load to a point of diminishing returns at about  $d=\lambda/2$ . At this value of  $d$ , 96% of the limiting load is achieved. In contrast, Backers [4] and Yonnet [1] have recommended  $d=\lambda$ . Other design issues such as centrifugal forces on rotors, bending stiffnesses of rotors and stators, and durability in assembly, should also be considered in choosing the radial bearing thickness.

Note that the load expression (11) is independent of spatial period,  $\lambda$ , when  $g$ ,  $x$  and  $d$  are scaled with  $\lambda$ . This means that the bearing gap and radial thickness can be reduced while maintaining the same peak load capability. The stiffness of the bearing increases with this scaling according to Eq. (13), but the ability of the bearing to absorb energy decreases as  $\lambda$  decreases. For most designs the nominal gap will be chosen slightly less than the peak load gap. The motivation for this is that the bearing stiffness can be increased substantially with only modest degradation of the peak load. The latter follows from the flatness of the Fig. 5 curves near the peak load dimensions. In selecting  $R$  and  $L$ , the primary objective is to provide enough journal area to achieve the desired load and stiffness requirements. Since our calculation neglects end-effects,  $L$  should be large enough so that there are 4 or 5 rings in the stack.

Finally, we reiterate two rules-of-thumb for design: the peak load of a stacked structure PM bearing fabricated using 42 MGOe magnetic material is roughly 0.4 MPa (60 psi) times the axial cross section of the bearing and the corresponding peak axial load is 0.6 MPa (85 psi) times the axial cross section.

## Acknowledgment

The authors are grateful to Dave Paden for providing the graphics for this manuscript. The research funding provided by the University of Pittsburgh Artificial Heart Program and the Bill and Susan McGowan Foundation is also gratefully acknowledged.

## References

- [1] Yonnet, J. P., Lemarquand, G., Hemmerlin, S., and Olvierrulliere, E., 1991, "Stacked Structures of Passive Magnetic Bearings," *J. Appl. Phys.*, **70**(10), pp. 6633–6635.
- [2] Antaki, J., Banda, S., Paden, B., and Piovoso, M., 2002, "Award Winning Control Applications," *IEEE Control Syst. Mag.*, **22**(6), December, pp. 8–20.
- [3] Baermann, M., 1956, German patent application B 30 042 dated 1954 (German specification 1071 871).
- [4] Backers, F. T., 1960–1961, "A Magnetic Journal Bearing," *Philips Tech. Rev.*, **22**, pp. 232–238.
- [5] Yonnet, J. P., 1978, "Passive Magnetic Bearings With Permanent Magnets," *IEEE Trans. Magn.*, **14**(5), pp. 803–805.
- [6] Yonnet, J. P., 1981, "Permanent Magnet Bearings and Couplings," *IEEE Trans. Magn.*, **17**(1), pp. 1169–1173.
- [7] Marinescu, M., and Marinescu, N., 1994, "A New Improved Method for Computation of Radial Stiffness in Permanent Magnet Bearings," *IEEE Trans. Magn.*, **30**(5), pp. 3491–3494.
- [8] Abramowitz, M., and Stegun, I. A., eds., 1964, *Handbook of Mathematical Functions*, Washington, DC; National Bureau of Standards.